Available online at www.sciencedirect.com
ScienceDirect
Journal of the European Ceramic Society 26 (2006) 3383–3391
www.elsevier.com/locate/jeurceramsoc

Effects of solvents on properties of nanocrystalline hydroxyapatite produced from hydrothermal process

Xingyuan Guo, Ping Xiao *

Materials Science Centre, School of Materials, University of Manchester, Grosvenor Street, Manchester M1 7HS, UK

Received 22 December 2004; received in revised form 16 September 2005; accepted 24 September 2005
Available online 22 November 2005

Abstract

Hydroxyapatite (HA) particles have been synthesised in isopropanol–water solvent via hydrothermal process. The influences of isopropanol on crystallisation, such as phase evolution, crystallite size, crystallinity degree, chemical composition, and agglomeration of the HA nanoparticles have been investigated by using XRD, FTIR, TEM, BET, TG-DSC and laser diffraction method. All HA nanoparticles prepared in the water–isopropanol mixed solvent have been found to be carbonated HA, and the amount of carbonate increased with increase of alcohol in the solvent. However, the crystallite size and crystallinity degree of the HA nanoparticles decreased with the addition of isopropanol. In addition, there was little change in morphology of HA particles produced in different solvents, though the aspect ratio of the HA increased slightly with increasing concentration of alcohol. The agglomeration was found to be mainly controlled by the zeta-potential and not by the change of solvent.

Keywords: Alcohol–water; Apatite; Biomedical application; Hydrothermal methods

1. Introduction

Synthesis of hydroxyapatite ($Ca_{10}(PO_4)_6(OH)_2$, HA) is of great importance for various industrial purposes, such as medicine, biology and fertilizer production.[1] So far, several techniques have been used for preparation of HA powder, which can be divided into two major routes: wet methods and solid-state reaction. The wet methods include co-precipitation,[2–4] hydrothermal process,[5–7] sol–gel synthesis,[8] mechanochemical method,[9,10] post-reaction refinement by emulsion.[11–13] Depending on the technique, materials with various morphologies, composition, and crystallinity degree have been obtained, which will essentially affect the bioactivity, mechanical properties and dissolution behavior in biological environment.[14,15] Therefore, it is becoming important to develop HA synthesis methods with precise control of particle size, morphology, crystallinity degree and chemical composition.

Hydrothermal process has been used to produce crystalline materials from solutions or sols into the desired crystalline phases at elevated temperature and pressure, typically at <350 °C and <150 atm. Particle size and morphology of products from hydrothermal process can be controlled by experimental conditions that regulate nucleation, growth and aging processes.[16] Nanocrystalline HA was reported to be prepared by hydrothermal methods with high crystallinity, homogeneity and close Ca/P ratio to 1.67 as in HA.[5,7,14] Our previous work showed that nanocrystalline HA was synthesized from hydrothermal processing in water.[17] However, the control of particle composition and crystallinity degree in aqueous solvent is poor.

Solvent effects on crystallite size, morphology, agglomeration and phase formation in solvo-thermal processing have been reported previously.[18,19] Physico-chemical properties of solvent, such as dielectric constant, interionic attraction, and the solute–solvent interaction strongly influence the solubility and diffusion behavior of the chemical precursors in the solvent. The addition of alcohol, e.g. isopropanol, could have a significant effect on the crystal growth, phase formation and particle agglomeration of synthesized materials. The effect of methanol on the morphology of HA crystals have been studied by Nagata et al. under hydrothermal conditions. The results indicated that only rod-like crystals about 20–100 nm in size formed without methanol and the addition of methanol increased the ratio of plate-like crystals, when add 50% methanol by weight, only

* Corresponding author. Tel.: +44 161 306 5941; fax: +44 161 306 3586.
E-mail address: ping.xiao@manchester.ac.uk (P. Xiao).

0955-2219/$ – see front matter © 2005 Elsevier Ltd. All rights reserved.
doi:10.1016/j.jeurceramsoc.2005.09.111

plate-like crystals 20–200 nm in size were observed.[7] Riman et al. reported that HA crystals synthesized in isopropanol (50%)–water solution had low aspect ratios ranging between 2 and 3.[14] Furthermore, our recent work indicated that the agglomeration of yttria-stabilized zirconia (YSZ) nanopowder synthesized in ethanol–isopropanol mixture solvent was hindered and a well-dispersed YSZ nano suspension was obtained. This result can not be explained by the DLVO theory but by solvation effect in alcohol solution.[19] In this article, the effects of isopropanol on crystallization of nanocrystalline HA were studied, in an attempt to control the crystallite properties and agglomeration.

2. Experiment procedures

2.1. Powder synthesis

Analytical pure $Ca(OH)_2$ and 85% H_3PO_4 were used as starting materials. 3.71 g (0.05 mol) $Ca(OH)_2$ was dispersed in 100 ml deionized water, and stirring for 5 h to form a uniform suspension. At the same time, 2 ml 85% H_3PO_4 (0.03 mol) was diluted by 8 ml deionized water. The ratio of Ca/P was kept at 1.67 as HA. Then the diluted H_3PO_4 solution was added to the $Ca(OH)_2$ suspension drop by drop while stirring gently (the dropping rate is about 1 ml/min). Finally a white calcium phosphate precursor (termed as HA precursor) was formed at the end of titration. For hydrothermal processing of the precursor, a fixed amount of precursor was centrifugally separated and redispersed in 0, 20, 50, 70 vol.% isopropanol in water, respectively. The HA precursor suspension in solvent was transferred to a 300 ml autoclave (pressure vessel), then placed in a mantle heater and treated hydrothermally at 220 °C for 10 h. A temperature program was used to control the heater around the external surface of the pressure vessel, while the actual reaction temperature was monitored using an internal thermocouple. The final product was washed in water and ethanol twice, respectively, and then vacuum filtered, dried in air for characterization.

2.2. Powder characterization

X-ray diffraction (XRD) analysis of powders was conducted using a Philips diffractometer (PW3710) with Cu Kα radiation over the 2θ range of 5–85° at room temperature with a step size of 0.02°. Infrared spectra (FTIR) of HA powders were obtained using Perkin-Elmer system 2000 spectrometer. Pellets for FTIR analysis were prepared from 1:150 HA–KBr mixtures (by weight), which were ground in a mortar and pestle for 15 min and pressed into pellets using a cold press. Thermal analysis was carried out on the powder by TG-DSC from 20 to 1200 °C in air atmosphere with a heating rate of 5 °C/min. Specific surface area measurements were made using the BET method utilizing adsorption of N_2 gas at −196 °C (Coulter SA3100 surface analyzer) after outgas at 250 °C for 15 min. Particle size distributions and mean particle sizes of samples were measured by Mastersizer microplus (Malvern Ltd., UK). Zeta potentials of those HA powders at various pH values have been examined by using the Coulter DELSA 440SX. For zeta-potential measurements, samples were prepared by diluting a 3 wt% stock suspension into 0.01 M KCl at pH 12 to obtain a working concentration of 0.03 wt%. Each suspension was titrated to various pH values and dispersed ultrasonically before analysis. The morphology of HA powders were determined by a transmission electron microscope (TEM, Philips, CM200) at 200 kV.

The crystallite size of the synthesized HA was calculated from the broadening in the XRD pattern. According to the Scherrer equation:[20]

$$t_{(hkl)} = \frac{0.9\lambda}{\beta \cos \theta_{(hkl)}}$$

where $t_{(hkl)}$ is the crystallite size, λ the wavelength of the monochromatic X-ray beam ($\lambda_{Cu} = 0.154056$ nm), β the full width at half maximum (FWHM), $\theta_{(hkl)}$ the peak diffraction angle and satisfies the Bragg's law for the ($h\,k\,l$) Miller's plane. To determine the full width at half maximum (FWHM) we used the basal reflection Miller's plane (0 0 2) peak since it is sharp and isolated from others. This peak also shows the crystal growth along the c-axis of the HA crystalline structure. In addition, the crystallite size based on the (3 0 0) Miller's plane, which indicates the crystal growth along the a-axis of HA, was also calculated in order to compare with that along (0 0 2). Meanwhile, crystallite size was also measured from the TEM images. The width and length of 50 crystals were measured from five randomly selected areas of each sample, average width and length was calculated from the measurements.

The measurement of crystallinity degree was performed with X-ray diffraction and infrared spectroscopy.[21] For XRD measurements, the crystallinity index (CI) for HA is based on the degree of resolution of the four X-ray reflection between 30° and 35° by using the semi-quantitative method of Person et al.: $CI = (h(2\,0\,2) + h(3\,0\,0) + h(1\,1\,2))/h(2\,1\,1)$ ($h(2\,0\,2)$ means the height of (2 0 2) reflection), which is more practical and more accurate than the classic measurement of the (0 0 2) reflection breadth at half-height.[22,23] The heights of the (2 0 2), (3 0 0) and (1 1 2) diffraction peaks were measured between the average value of distance between the top of the peak and the 'valley' separating it from the next peak (illustrated in Fig. 1A). $h(2\,1\,1)$ is the height of the highest peak (2 1 1), subtracting the value of the baseline taken between 24° and 38° of 2θ. The CI was given as the average value of three measurements with an error of ±0.01.

For FTIR measurements, the splitting factor (SF) as an indication of crystallinity was calculated using the method given by Weiner and Bar-Yosef.[24] After a baseline correction between 495 and 750 cm^{-1}, the intensity of the two $\gamma_4(PO_4)^{3-}$ vibration bands at 605 cm^{-1} (a) and 565 cm^{-1} (b) in the absorbance mode was measured and their sum was then divided by the intensity (c) of the valley between these absorption bands above the baseline; i.e. $SF = (a + b)/c$ (illustrated in Fig. 1B). Higher is the value of CI or SF, higher is the crystallinity degree.

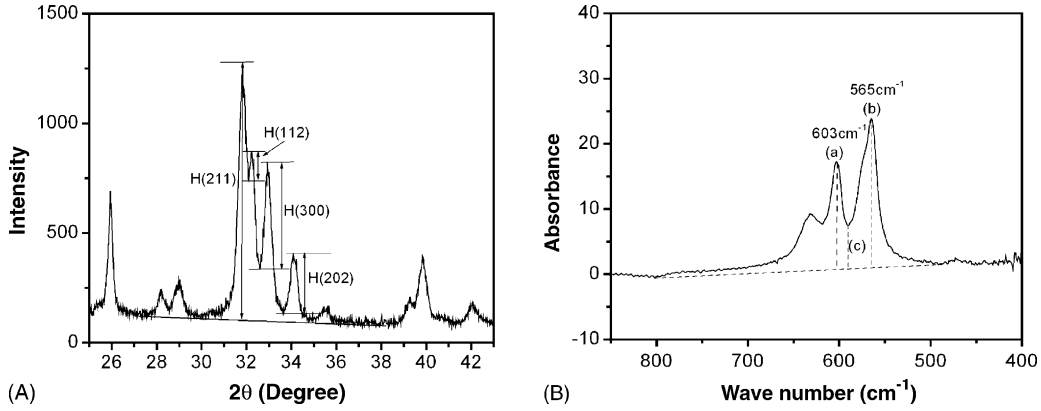

Fig. 1. Schematic figures of (a) XRD, (b) FTIR spectra for calculating (A) crystallinity index (CI); and (B) splitting factor (SF), respectively. See Section 2.2 for detailed description.

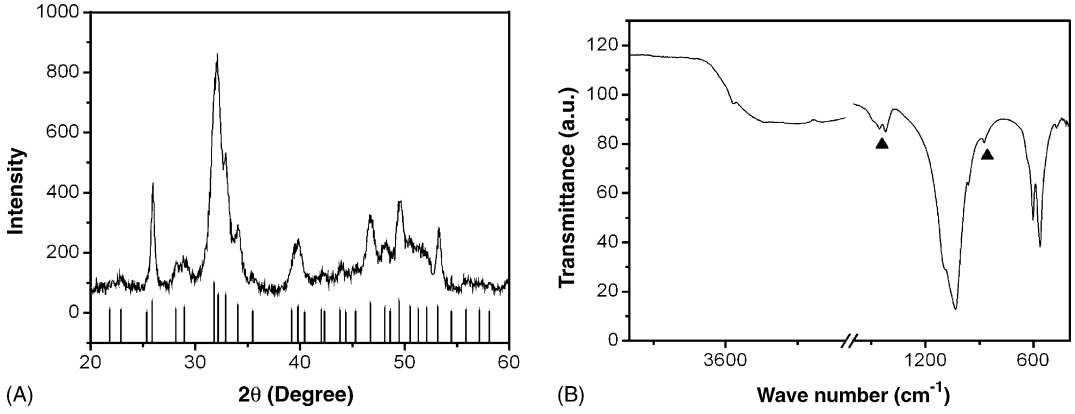

Fig. 2. (A) XRD pattern of the HA precursor before hydrothermal treatment in comparison to ASTM 9-432 file data for HA. (B) FTIR spectrum of the HA precursor before hydrothermal treatment ((▲) absorption due to $(CO_3)^{2-}$).

3. Results

3.1. Crystalline structure and composition of HA precursor

Fig. 2 shows X-ray diffraction pattern and FTIR spectrum of HA precursor prepared in pure water before hydrothermal process. X-ray diffraction pattern in Fig. 2A indicated that HA precursor is a single phase HA compared with the ASTM 9-432 file data for HA. However, the crystallinity degree of the HA precursor was low with a crystallinity index of 0.21. The average crystallite size (t_{002}), determined from X-ray broadening analysis, is about 20 nm. Fig. 2B shows the bonding analysis of the HA precursor by FTIR in a range of 400–4000 cm^{-1}. This FTIR spectrum is consistent with the data from hydroxyapatite synthesized by other methods.[25,26] Most of the peaks are attributed to three vibration modes: (1) three $(PO_4)^{3-}$ stretching modes occurring at 961 (γ_1), 1033 and 1092 cm^{-1} (γ_3), and two $\gamma_4(PO_4)^{3-}$ bending modes at 563, 602 cm^{-1}; (2) the stretching modes of $(CO_3)^{2-}$ occurring at 873 (γ_2), 1421 and 1457 cm^{-1} (γ_3); and (3) the stretching mode of OH^- occurring at 3572 and 633 cm^{-1}, which is so weak that only shown as a small shoulder. H–O–H peak was also observed at 3410 and 1636 cm^{-1}. The spectrum suggests that HA precursor produced by precipitation is carbonate containing HA. The relative carbonate amount estimated by integrated area ratio of absorption band due to carbonate in the range of 1380–1600 cm^{-1} (γ_3CO_3) and phosphate group in the range of 970–1083 cm^{-1} (γ_3PO_4),[27] was 0.11.

3.2. HA particles after hydrothermal treatment

3.2.1. Crystalline structure

Fig. 3 shows the X-ray diffraction patterns of the HA powders after hydrothermal treatment in the water–isopropanol mixed solvent. Comparing Fig. 3 with Fig. 2A, there is no forma-

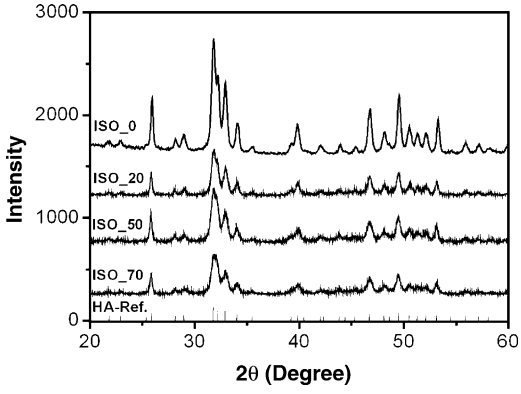

Fig. 3. XRD pattern of hydroxyapatite treated in different reaction media during hydrothermal process in comparison to ASTM 9-432 file data for HA.

Table 1
Calculated lattice parameters for all HA particles synthesized in various media

Sample code	ISO_0	ISO_20	ISO_50	ISO_70
Vol.% of 2-propanol	0	20	50	70
Lattice parameter: a (Å)	9.417	9.416	9.413	9.413
Δa	−0.001	−0.002	−0.005	−0.005
Lattice parameter: c (Å)	6.879	6.883	6.885	6.886
Δc	−0.005	−0.001	+0.001	+0.002
Unit cell volume: V (Å^3)	1584.86	1585.44	1584.89	1585.12
ΔV	−1.48	−0.90	−1.45	−1.22

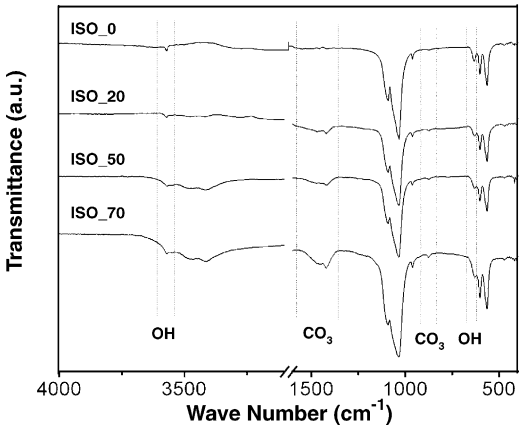

Fig. 4. Infrared spectra of hydroxyapatite synthesized in different media.

tion of new phase except for crystallization of HA during hydrothermal process. All of peaks correspond to HA phase only, which are consistent with the ASTM 9-432 file data for HA ($a = b = 9.418$ Å, $c = 6.884$ Å, symmetry group $P6_3/m$). The resolved peaks of (2 1 1), (1 1 2) and (3 0 0) indicate an increased crystallinity degree. As can been seen in Fig. 3, the intensity of X-ray pattern decreased with increasing concentration of isopropanol, which suggested a decreased crystallinity degree when treated in isopropanol–water mixed solvent. The lattice parameters a, c and hexagonal volume of cell unit of all HA powders calculated using CELREF software were presented in Table 1. With respect to reference HA (9-432), the lattice a decreased for all samples, while the lattice c increased for samples produced in ISO_50 (isopropanol% in solvent = 50%), ISO_70, and decreased for sample produced in ISO_0 and ISO_20. The total unit cell volume decreased almost 0.1% for all samples.

The FTIR analysis results for HA particle after hydrothermal treatment in different solvents (as shown in Fig. 4) were similar to that for HA precursor except for the increased absorption intensity of O–H band at 3572 and 633 cm^{-1}, which can be attributed to the increased crystallinity degree. A decreasing intensity of O–H band at 633 cm^{-1} has been observed with increasing the isopropanol concentration from 0 to 70%, which suggested a decreased crystallinity or an increased carbonate substitution in OH position as type A. An interesting phenomenon was the absence of (CO_3^{2-}) absorption peaks for the sample produced in water. The relative carbonate amount in the form of integrated area of $\gamma_3CO_3/\gamma_3PO_4$ decreased from 0.11 in the HA precursor before hydrothermal process to 0 in the sample produced in water, i.e. ISO_0, whereas it increased to 0.25 in the sample produced in the ISO_70 as shown in Table 2.

From the XRD pattern and FTIR spectra, an increased crystallinity after hydrothermal treatment is obvious. In order to semi-quantify the crystallinity degree among those samples after hydrothermal treatment in different media, the methods described in Section 2 has been used. As shown in Table 2, hydrothermal process in water increased the crystallinity index from 0.21 to 0.7, whereas with increasing the isopropanol concentration from 0 to 70% crystallinity index decreased from 0.7 to 0.58, and splitting factor decreased from 7.51 to 5.49.

3.2.2. Thermal behavior

The features of TG profile of HA powders prepared in various media are presented in Fig. 5. Two endothermic peaks around 380 and 780 °C were observed due to dehydration and decomposition. The weight loss could be differentiated into four regions in the investigated temperature range such as (1) 20–250 °C, (2) 250–400 °C, (3) 400–780 °C, (4) 780–1200 °C according to Markovic et al.[28] and Landi et al.[29]. The weight loss below 250 °C was mainly attributed to the loss of physisorbed water. Between 250 and 400 °C, a severe weight loss was observed which is attributable to the elimination of chemisorbed water and other absorbed species such as CO_2. The weight loss from 20 to 400 °C as shown in Table 2 increased from 3.12 to 5.94% when

Table 2
Details of all HA powders synthesized in various media

Sample code	Precursor	ISO_0	ISO_20	ISO_50	ISO_70
Relative carbonate amount in $\gamma_3CO_3/\gamma_3PO_4$	0.11	0	0.14	0.18	0.25
Crystallinity index (CI)	0.21	0.70	0.68	0.64	0.58
Splitting factor (SF)	–	7.51	6.29	5.61	5.49
Weight loss 20–400 °C (%)	7.96	3.12	4.99	5.06	5.94
Weight loss 780–1200 °C (%)	1.11	0.80	1.79	1.71	1.90
Specific surface area (cm^2/g)	98.5	46.9	82.0	75.6	73.9

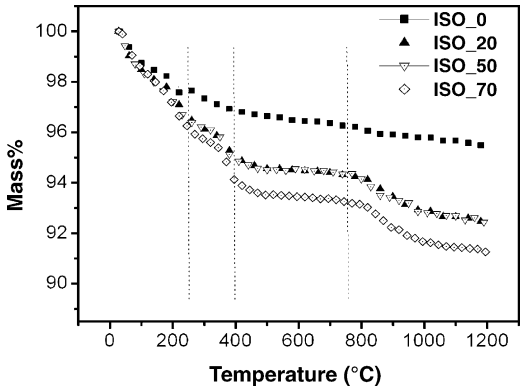

Fig. 5. Thermal behaviour of hydroxyapatite synthesized in different media.

increasing isopropanol concentration from 0 to 70%, which might be attributed to the high absorption of water and CO_2 from atmosphere. In order to confirm that, surface areas were measured by BET, which is shown in Table 2. The ISO_0 sample got the lowest specific surface area 46.9 m^2/g, while others are 1.5 time of ISO_0 (70–80 m^2/g)). Such different caused the different amount of absorbed water and CO_2, and subsequently different weight loss when heating up.

The weight loss from 400 to 780 °C was quite small for all samples, which mainly corresponded to water loss from HPO_4^{2-}/$P_2O_7^{4-}$/HA/β-TCP reactions, such as

$$2HPO_4^{2-} \rightarrow P_2O_7^{4-} + H_2O$$

$$P_2O_7^{4-} + 2OH \rightarrow 2PO_4^{3-} + H_2O$$

Since the amount of HPO_4^{2-} is small, the weight loss at this stage can be neglected. The weight loss after 780 °C was mainly due to the decomposition of carbonate. At this stage, the weight loss increased from 0.80 in ISO_0 to 1.90 in ISO_70 when increasing the isopropanol concentration, which meant that the amount of carbonate increased with the increase of isopropanol concentration, such trend is consistent to the trend of relative carbonate amount calculated by FTIR.

3.2.3. Morphologies and crystallite size

Fig. 6 shows the TEM micrographs and diffraction pattern of HA produced in different media. All TEM images show relatively uniform particles with a rod-like shape. All the diffraction patterns are similar to the pattern shown in Fig. 6e. With a SAD aperture of 100 nm diameter, the multi-spot rings of the SAD pattern for both samples indicated nano-crystalline HA. The HA particles produced in the mixed solvent tended to be damaged under illumination of electron beam, suggesting the lower crystallinity, in comparison samples prepared in water, which is consistent with the XRD and FTIR results. The crystallite size was measured based on examination of TEM images and analysis of XRD peaks using Scherrer equation. Table 3 shows the effect of isopropanol on the crystallite sizes. The crystallite size along *c*-axis (termed as t_{002}) obtained from analysis of (0 0 2) broadening slightly decreased from 56.8 to 44.3 nm, and the crystallite size along *a*-axis (termed as t_{300}) decreased from 28.5 to 16.7 nm with increasing the isopropanol volume concentration from 0 to 70%. The rod length and diameter measured from TEM images appeared to give similar trend, i.e. rod length decreased from 77 ± 21 to 58 ± 11 nm with the increase of isopropanol volume concentration from 0 to 70%, and the rod diameter decreased from 26 ± 2 to 16.7 ± 2.7 nm with the increase of isopropanol concentration from 0 to 70%. Our previous work indicated that *c*-axis is parallel to the length of the HA rods,[17] which means t_{002} is related to the length of the rod, while t_{300} is related to the diameter of the rod. According to Table 3, the diameter of the rod is very close to t_{300} measured using XRD. But the rod length is larger than t_{002}, which might be due to the inaccuracy in both XRD analysis and TEM image examination. However, the ratio of length/diameter and t_{002}/t_{300} increased from 2.98 to 3.52, and 1.99 to 2.66, respectively, with increase in isopropanol concentration from 0 to 70%.

3.2.4. Agglomeration and particle size distribution

Particle size distribution measured using laser diffraction is a main indication of particle agglomeration. The agglomerate/aggregate size was measured as the hydrodynamic diameter distribution in water at pH 10. Fig. 7 shows the agglomerate size of powders prepared in different reaction media. Mixed isopropanol–water solvents did not have significant effect on agglomeration. However, the particle size of HA powder prepared in 70% isopropanol was slightly less than others.

The zeta potential represents the formation of a double charge layer at the surface of particles, which induce electrostatic repulsive forces between particles hindering the agglomeration of the ceramic suspension. Fig. 8 shows the zeta potential of the HA suspension as function of pH values. It can be seen that the isoelectric points (IEP) are at pH 8.7, pH 8.2, pH 8.7, and pH 11.1 for ISO_0, ISO_20, ISO_50, and ISO_70, respectively. At the IEP, the zeta potential is zero; therefore, the repulsion force is at its minimum and colloid particles can agglomerate easily. The zeta potential for ISO_0, ISO_20, and ISO_50 at pH 10 is about −5 mV, while for ISO_70 is about +10 mV.

Table 3
Crystallite size of all HA particles measured by XRD and TEM

Sample code	ISO_0	ISO_20	ISO_50	ISO_70
Length by TEM (*L*)	76.9 ± 20.5	70.6 ± 20.1	58.8 ± 8.4	57.9 ± 11.5
Diameter by TEM (*D*)	25.8 ± 1.5	21.2 ± 5.4	17.1 ± 3.0	16.7 ± 2.7
Ratio of (*L*/*D*)	2.98	3.33	3.44	3.52
t_{002}	56.8 ± 1.0	54.9 ± 2.0	46.9 ± 1.0	44.4 ± 3.0
t_{300}	28.5 ± 0.2	21.4 ± 0.5	17.9 ± 1.5	16.7 ± 0.3
Ratio of (t_{002}/t_{300})	1.99	2.57	2.62	2.66

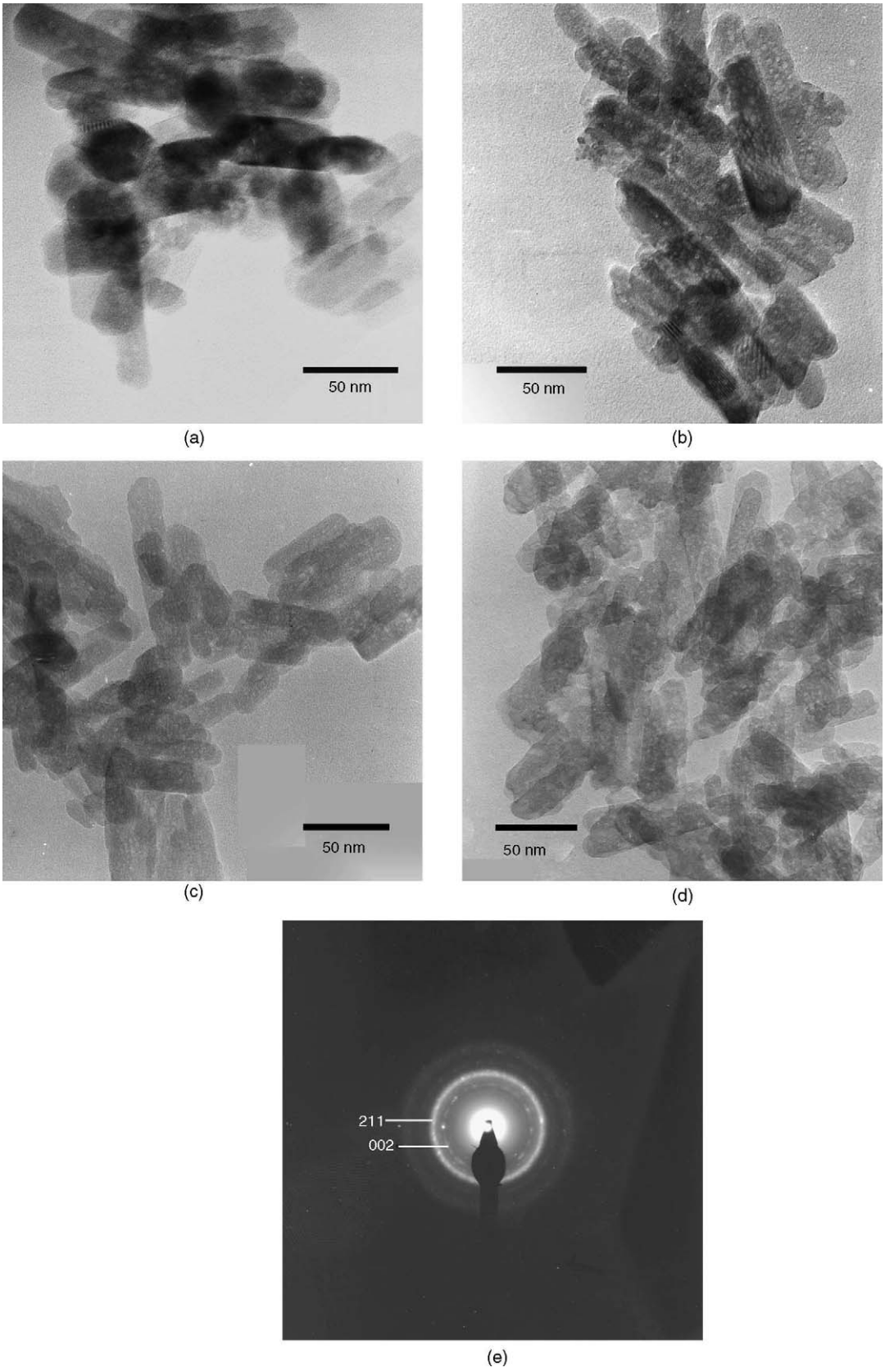

Fig. 6. Morphology of hydroxyapatite particles synthesized in different media: (a) ISO_0; (b) ISO_20; (c) ISO_50; dISO_70; (e) diffraction pattern of ISO_50.

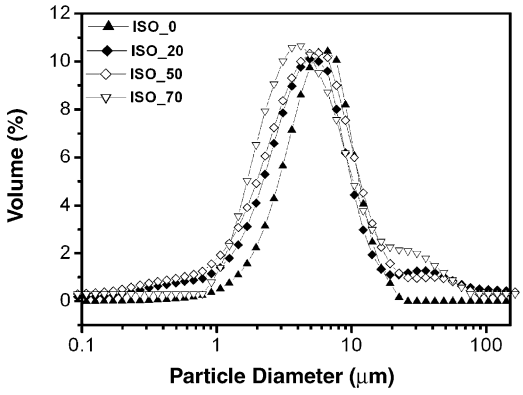

Fig. 7. Particle size distribution of hydroxyapatite after treated in different media measured at pH 10.

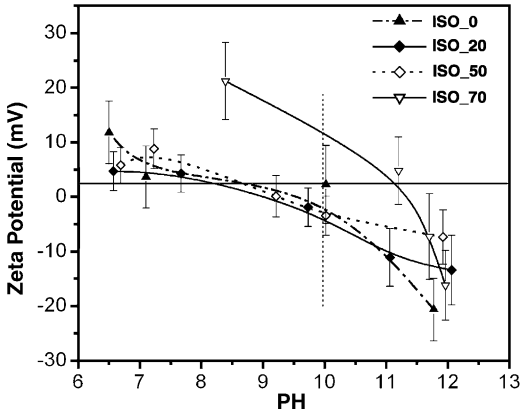

Fig. 8. Zeta potential of hydroxyapatite synthesized in different media as a function of pH, the concentration for measurement is about 0.03 wt%.

4. Discussion

It is well known that biological apatite contains carbonate ions in different sites; one is the Type A carbonate hydroxyapatite in which CO_3^{2-} ions are substituted for OH^- ions, and the other is the Type B in which CO_3^{2-} ions are substituted for PO_4^{3-} ions.[28,30] A common method of determining the type of carbonated substitution is to examine the positions of carbonate bands observed in FTIR spectra. However, many different studies have resulted in contradictory explanations regarding which bands correspond to Type A, Type B or mixed Type AB carbonate substitution.[15,28,31,32] The HA powder in this study presented carbonate bands at 1457, 1421, and 873 cm^{-1}, which is in agreement with the study of Tinti and co-workers as Type B substitution, whereas the Type A bands locate at 1550, 1457, and 880 cm^{-1}.[32] Further evidence to determine where the substitution occurs is the deviations of unit cell parameters. Gibson and Bonfield[15] and Astala and Stott[30] have shown that the *a*-axis decreases and the *c*-axis increases or slightly changes with increasing carbonate substitution as Type B, with the reverse occurring for substitution as Type A. The decrease in the lattice a and that in the lattice c for those HA powder prepared in different solvents (Table 1) suggest that carbonate ion substitution occurred on phosphate site as Type B. The behaviour of the lattice a can be explained by considering that the carbonate ion is larger than the hydroxyl ion but smaller than phosphate ion; therefore, it expand *a*-axis when replacing hydroxyl site (Type A), whereas reduce the *a*-axis when replacing the phosphate site (Type B). Furthermore, for most stable structures, the unit cell volumes increased by 2.6% for Type A carbonate substitution, and decreased by 1.1–3.3% for Type B carbonate substitution.[30] In our case, all unit cell volumes decreased by 0.5%, which indicates a Type B carbonate substitution, though the unit cell volume decrease is smaller than Stott's.

Besides the carbonate substitution site, carbonate amount of HA powder prepared in various solvents was studied by different analytical methods. Both FTIR spectrum and XRD results showed that HA precursor contains carbonate. The carbonate was mainly from CO_2 dissolved in the $Ca(OH)_2$ suspension previous to the H_3PO_4 addition. However, the relative carbonate amount of HA powder in the form of $\gamma_3CO_3/\gamma_3PO_4$ decreased after hydrothermal treatment in pure water, while increased after hydrothermal treatment in alcohol–water mixed solvent, which can be further confirmed by TG analysis. The weight loss of HA powder in the range of 780–1200 °C, which was mainly due to decomposition of carbonate, decreased after hydrothermal treatment in pure water, while increased after hydrothermal treatment in isopropanol–water mixed solvent. The reason why alcohol–water mixed solvent influenced the carbonate amount in HA powder is uncertain. We propose that a process involving dissolution–crystallisation might account for this.[14] The solubility product can be represented by K_{sp}. The $-\log(K_{sp})_{25^\circ}$ (at 25 °C) of amorphous calcium phosphate (ACP) and pure hydroxyapatite is 25.7–32.7 and 118.6, respectively.[33] The higher the $-\log(K_{sp})_{25^\circ}$ is, the lower solubility is. In this study, we assume that the $-\log(K_{sp})_{25^\circ}$ of our HA precursor is slightly higher than that of ACP, but much lower than that of pure HA. Therefore, in pure water, the high crystalline HA was formed via dissolution of the HA precursor and precipitation of crystalline HA. Furthermore, it has been reported that the $-\log(K_{sp})_{25^\circ}$ of carbonated HA decrease with the increase of carbonate amount. Itoh et al.[34] has obtained a formula to describe the relationship of solubility product between pure HA and carbonated HA as follows

$$pK_{sp} = -\log K_{sp} = 118.65 - 0.47316\,CO_2\,(wt\%)^{2.4176} \quad (1)$$

So the carbonated HA dissolved in water and formed purer HA after the hydrothermal process. In alcohol–water mixed solvent, the solubility of HA precursor decreased since HA is a polar molecular, consequently decreased dissolution, and resulted in a decrease of HA re-crystallisation. So the transformation of the HA precursor to pure crystalline HA via dissolution and precipitation was hindered.[1] In addition, the formation of carbonated apatite is kinetically favoured, according to Biostelle and Lopez-Valero,[35] which claimed that nucleation is easier for highly soluble crystalline species if all other conditions are same.

Although the crystallinity degree and crystallite size increased after hydrothermal treatment, with the increase of isopropanol volume concentration, the crystallinity degree and crystallite size decreased, as the dissolution and precipitation process was hindered by the presence of alcohols. Previous studies have confirmed that with increasing carbonate content, the

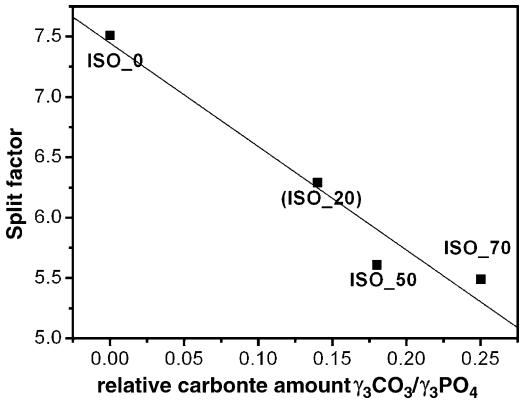

Fig. 9. Splitting factor as a function of relative carbonate amount.

apatitic structure becomes progressively more amorphous.[32,36] Tinti and coworkers[32] has reported that the crystallinity, which was expressed as full width at half maximum at 962 cm^{-1} ($FWHM_{962}$) based on Raman spectra, decreased linearly with the carbonate amount. In our case, the crystallinity in a form of splitting factor decreased almost linearly with the relative carbonate amount, which was expressed as ratio of integrated area of $\gamma_3CO_3/\gamma_3PO_4$ (shown in Fig. 9).

Although the HA particles showed nano-scale crystallite, the agglomerate size is in micron range. According to DLVO theory, the barrier for agglomeration in solvent can be calculated as follows.[19]

$$V = -\frac{Aka}{12} + 2\pi\varepsilon_0\varepsilon_r a\Psi^2 \quad (2)$$

where V is the energy barrier for aggregation/agglomeration between two particles, a the particle diameter, A the effective Hamaker constant, k the Debye-Huckel parameter, ε_0 and ε_r the dielectric constant of vacuum and the medium solvent, and Ψ is the surface potential. The Debye-Huckel parameter is defined by Eq. (3)

$$k = \left(\frac{2F^2Z^2C}{\varepsilon_0\varepsilon_r k_B T}\right)^{1/2} \quad (3)$$

where F is the electrical charge (96 500 C), k_B the Boltzmann constant, Z the ionic valence, and C is the concentration of the electrolyte. The effective Hamaker constant depends on the dispersion medium.

The addition of alcohol to water changed both electrolyte concentration C and dielectric constant. The dielectric constants for water and isopropanol are 80 and 17.9, respectively. It appeared that the change of agglomerate size from the 20% isopropanol addition to the 50% isopropanol addition had little effect on agglomerate size. This results suggest that either the decrease in dielectric constant balanced the effect of the decrease in electrolyte concentration, according to Eq. (3) or the effect of dielectric constant change and electrolyte concentration change is not significant enough due to presence of solvation films which can not be predicted using the DVLO theory.[19] On the other hand, the 70% isopropanol addition did have some effect on the agglomerate size in comparison with other solvents, particularly in comparison with water as solvent. According to Fig. 8, the zeta-potential showed significant difference between the particles in 70% isopropanol solvent and that in the other solvents. At pH value of 10 at which the agglomerate size was measured, the zeta-potentials for 20–50% isopropanol are very similar (∼−5 mV). However, the zeta-potential for the 70% isopropanol is above 10 mV whereas the zeta potential for water is about 0 mV. These results are clearly in agreement with the prediction of agglomeration based on Eq. (2).

5. Conclusions

The addition of isopropanol to water as solvent influenced the chemical composition and crystallinity degree of HA particles. It was found that the carbonate amount increased with increasing of isopropanol concentration, while crystallinity decreased with increase isopropanol. However, the solvent has little effects on morphology and agglomeration of HA particles, although the 70% isopropanol addition reduced the particle/agglomerate size slightly. The formation mechanism of HA in mixed solvent is similar to that in pure water, which involved both dissolution and re-crystallisation process. Further studies are needed to confirm the effect of solvent alone on crystallinity by prepare HA without carbonate.

References

1. Tung, M. S. and O'Farrell, T. J., Effect of ethanol on the formation of calcium phosphates. *Colloids Surf. A*, 1996, **110**, 191.
2. Koumoulidis, G. C., Vaimakis, T. C. and Sdoikos, A. T., Preparation of hydroxyapatite lathlike particles using high-speed dispersing equipment. *J. Am. Ceram. Soc.*, 2001, **84**(6), 1203.
3. Tadic, D., Peters, F. and Epple, M., Continuous synthesis of amorphous carbonated apatites. *Biomaterials*, 2002, **23**, 2553.
4. Kong, L. B., Ma, J. and Boey, F., Nanosized hydroxyapatite powders derived from coprecipitation process. *J. Mater. Sci.*, 2002, **37**, 1131.
5. Yoshimura, M., Suda, H., Okamoto, K. and Ioku, K., Hydrothermal synthesis of needle-like apatite crystal. *J. Ceram. Soc. Jpn.*, 1991(10), 1402.
6. Andres-Verges, M., Fernandez-Gonzalez, C. and Martinez-Gallega, M., Hydrothermal synthesis of calcium deficient hydroxyapatites with controlled size and homogeneous morphology. *J. Eur. Ceram. Soc.*, 1998, **18**, 1245.
7. Nagata, F., Yokogawa, Y., Toriyama, M., Kawamoto, Y., Suzuki, T. and Nishizawa, K., Hydrothermal synthesis of hydroxyapatite crystals in the presence of methanol. *Nippon Seramikkusu Kyokai Gakujutsu Ronbunshi-J. Ceram. Soc. Jpn.*, 1995, **103**(1), 70.
8. Nemoto, R., Nakamura, S., Isobe, T. and Senna, M., Direct synthesis of hydroxyapatite-silk fibroin nano-composite sol via a mechanochemical route. *J. Sol–Gel Sci. Technol.*, 2001, **21**(12), 7.
9. Pavel, S., Wojciech, L. S., Hao, T., Gulliver, E., Riman, R. E., TenHuisen, K. S. *et al.*, Mechanochemical–hydrothermal preparation of crystalline hydroxyapatite powders at room temperature. *J. Mater. Res.*, 2001, **16**(5), 1231.
10. Yeong, K. C. B., Wang, J. and Ng, S. C., Mechanochemical synthesis of nanocrystalline hydroxyapatite from CaO and $CaHPO_4$. *Biomaterials*, 2001, **22**, 2705.
11. Lim, G. K., Wang, J., Ng, S. C. and Gan, L. M., Nanosized hydroxyapatite powders from microemulsions and emulsions stabilized by a biodegradable surfactant. *J. Mater. Chem.*, 1999, **9**, 1635.
12. Lim, G. K., Wang, J., Ng, S. C. and Gan, L. M., Formation of nanocrystalline hydroxyapatite in nonionic surfactant emulsion. *Langmuir*, 1999, **15**, 7472.

13. Sonoda, K., Furuzono, T., Walsh, D., Sato, K. and Tanaka, J., Influence of emulsion on crystal growth of hydroxyapatite. *Solid State Ionics*, 2002, **151**(1–4), 321.
14. Riman, R. E., Suchanek, W. L., Byrappa, K., Chen, C. W., Shuk, P. and Oakes, C. S., Solution synthesis of hydroxyapatite designer particulates. *Solid State Ionics*, 2002, **151**(1–4), 393.
15. Gibson, I. R. and Bonfield, W., Novel synthesis and characterisation of an AB-type carbonate-substituted hydroxyapatite. *J. Biomed. Mater. Res.*, 2002, **59**, 697.
16. Wojciech Suchanek, M. Y., Processing and properties of hydroxyapatite-based biomaterials for use as hard tissue preplacement implant. *J. Mater. Res.*, 1998, **13**(1), 94.
17. Guo, X., Xiao, P., Liu, J. and Shen, Z., Fabrication of nanostructured hydroxyapatite via hydrothermal synthesis and spark plasma sintering. *J. Am. Ceram. Soc.*, 2004, **88**(4), 1026.
18. Chen, S., Yu, S. H., Yu, B., Ren, L., Yao, W. and Coifen, H., Solvent effect on mineral modification: selective synthesis of cerium compounds by a facile solution route. *Chem. Eur. J.*, 2004, **10**, 3050.
19. Wang, X. M., Lorimer, G. and Xiao, P., Solvothermal synthesis and processing of yttria-stabilized zirconia nanopowder. *J. Am. Ceram. Soc.*, 2004, **88**(4), 809.
20. Bouyer, E., Gitzhofer, F. and Boulos, M. I., Morphological study of hydroxyapatite nanocrystal suspension. *J. Mater. Sci. Mater. Med.*, 2000, **11**(8), 523.
21. Gross, K. A., Phillips, M., Ben-Nissan, B. and Berndt, C. C., Identification of the amorphous phase in plasma sprayed apatite coatings. *Bioceramics*, 1998, **11**, 177.
22. Person, A., Bocherens, H., Mariotti, A. and Renard, M., Diagenetic evolution and experimental heating of bone phosphate. *Palaeogeography Palaeoclimatol. Palaeoecol.*, 1996, **126**, 135.
23. Reiche, I., Vignaud, C. and Menu, M., The crystallinity of ancient bone and dentine: new insights by transmission electron microscopy. *Archaeometry*, 2002, **44**(3), 447.
24. Weiner, S. and Bar-Yosef, O., States of preservation of bone from prehistoric sites in the near East: a survey. *J. Archaeol. Sci.*, 1990, **17**, 187.
25. Luo, P. and Nieh, T. G., Preparing hydroxyapatite powders with controlled morphology. *Biomaterials*, 1996, **17**, 1959.
26. Panda, R. N., Hsieh, M. F., Chung, R. J. and Chin, T. S., FTIR, XRD, SEM and solid state NMR investigations of carbonate-containing hydroxyapatite nano-particles synthesized by hydroxide-gel technique. *J. Phys. Chem. Solids*, 2003, **64**, 193.
27. Corrand, D. M., *The effects of some biochemicals on the precipitation behavior of hydroxyapatite*. Department of Materials, The University of Oxford, Oxford, 1998.
28. Markovic, M., Fowler, B. O. and Tung, M. S., Preparation and comprehensive characterisation of a calcium hydroxyapatite reference material. *J. Res. Inst. Stand. Technol.*, 2004, **109**, 553.
29. Landi, E., Tampieri, A., Celotti, G., Vichi, L. and Sandri, M., Influence of synthesis and sintering parameters on the characteristics of carbonate apatite. *Biomaterials*, 2004, **25**, 1763.
30. Astala, R. and Stott, M. J., First principles investigation of mineral component of bone: CO3 substitutions in hydroxyapatite. *Chem. Mater.*, 2005, **17**(16), 4125–4133.
31. Chow, L. C., Sun, L. and Hockey, B., Properties of nanostructured hydroxyapatite prepared by a spray drying technique. *J. Res. Inst. Stand. Technol.*, 2004, **109**, 543.
32. Krajewski, A., Mazzocchi, M., Buldini, P. L., Ravaglioli, A., Tinti, A., Taddei, P. *et al.*, Synthesis of Carbonated hydroxyapatites: efficiency of the substitution and critical evaluation of analytical methods. *J. Mol. Struct.*, 2005, **744–747**, 221.
33. Oorozhkin, S. V. and Epple, M., Biological and medical significance of calcium phosphates. *Angew. Chem.*, 2002, **41**, 3130.
34. Itoh, A., Maekawa, K., Tsutsumi, S., Ikazaki, F. and Tateishi, T., Solubility product of OH-carbonated hydroxyapatite. *J. Biomed. Mater. Res.*, 1997, **36**, 552.
35. Boistelle, R. and Lopez-Valero, I., Growth unit and nucleation: the case of calcium phosphates. *J. Crystal Growth*, 1990, **102**, 609.
36. Baig, A. A., Fox, J. L., Hsu, J., Wang, Z., Otsuka, M., Higuchi, W. I. *et al.*, Effect of carbonate content and crystallinity on the metastable equilibrium solubility behavior of carbonated apatites. *J. Colloid Interface Sci.*, 1996, **179**, 608–617.